02;13

The ion–solid interaction potential determination from the backscattered particles spectra

© P.Yu. Babenko, A.N. Zinoviev, V.S. Mikhailov, D.S. Tensin, A.P. Shergin

Ioffe Institute, St. Petersburg, Russia
E-mail: zinoviev@inprof.ioffe.ru

Received April 22, 2022
Revised April 22, 2022
Accepted May 26, 2022

The values of the atomic particle–solid potential were obtained for the first time from experimental data on the energy spectra and angular dependences of backscattered particles. The proposed procedure for determining the potential has never been applied previously. It is shown that the obtained data do not depend on the potential approximation used. The ion–solid interaction potential differs markedly from the potential describing collisions in the gas phase. The screening constant increases by 10–15%. The increase in screening is due to an increase in the density of the electron gas in the region between the incident particle and scattering center.

Keywords: interatomic interaction potential, energy spectra, scattering of atomic particles on the surface.

DOI: 10.21883/TPL.2022.07.54039.19231

Data on the potential decisively affect the results of modeling such processes as particle reflection from the surface and passage through thin films, as well of modeling particle ranges, sputtering, and energy release. It is important to consider these processes in defining the plasma particles interaction with the Tokamak reactor first wall, in modeling ion implantation, and in analyzing the results of determining the near–surface layer characteristics based on ion and atom scattering. Data on potentials directly define nuclear stopping during the atomic particle beams transmission through matter.

In modeling collisions between atomic particles and solids, screened Coulomb potentials are used most often: Moliere potential [1], ZBL (Ziegler–Biersack–Littmark) potential [2], Lenz–Jensen potential [3,4], and Kr–C potential [5]. Paper [6] has proposed a potential that at present describes the experiments on gas–phase particle scattering best of all. In [7], calculations obtained in the density functional (DFT) approximation by using the Dmol code for choosing the wave function basis were compared with the experimental potential data. A good agreement between the theory and experiment was gained. DFT potentials corrected for experimental data on the potential–well parameters were successfully used in modeling coefficients of particle reflection from different targets [8] and calculating nuclear stopping power [9]. Some authors try to account for the influence of particle–solid interaction peculiarities in developing potentials to be used in calculations by the molecular dynamics method [10–12].

It was noticed that, in modeling energy spectra of scattered particles using computer codes, it is necessary to correct the screening constant in the potential so as to ensure better agreement with experiments [13]. In our work [14] devoted to studying the effect of rainbow scattering of atoms from metal crystal surfaces, we have derived from experimental data interaction potentials for a great number of systems; those potentials significantly differ from potentials commonly used to describe gas–phase scattering. This effect was explained by the influence of a charge induced in metal by the projectile atom [14]. Similar influence was revealed also in [15] in describing semi–channeling of N_2^+ ions on a copper crystal. Contrary to the case of gas phase, deriving the potential from the experiment on collisions in solids is hindered by the influence of multiple scattering and stopping of particles and also by changes in particle charges in passing through solids. Earlier no attempts have been made to acquire information on the potential by simulating energy and angular spectra of backscattered particles.

To describe particles scattering during bombardment of a solid, we used our own program code based on the Monte–Carlo method and binary collision approximation. The target was described via the microcrystalline model [16] that accounts for correlation in the arrangement of nearest neighbors by considering an atomic cluster one lattice constant in size. Position of the first atom and cluster orientation were chosen randomly. After the collision, a next cluster was created, which was arbitrary oriented in space. In our code, energy losses connected with scattering from target atoms were calculated exactly for the used interaction potential. Stopping on electrons was described by using the paper [17] data; correction for inelastic losses in collisions was calculated as a product of stopping power at the considered collision energy and the length of inter–collision trajectory. Thermal vibrations of the target atoms were taken into account.

Experimental data on the hydrogen ion scattering from gold were taken from [18]. The distinctive feature of that

Table 1. Parameters of the Zinoviev potential

Energy, keV	c_1	c_2	c_3	Error, %
5	1.954	1.120	0.017	6.8
8	1.875	1.123	0	8.5

Table 2. Parameters of the Moliere potential

Energy, keV	c_1	d_1	c_2	d_2	Error, %
5	0.462	0.427	0.5775	1.431	6.9
8	0.455	0.480	0.5775	1.536	8.9

experiment consisted in detecting all the scattered particles, both charged and neutral ones. This allowed elimination of the error arising due to an uncertainty in the fraction of charged particles in the total flux of scattered particles. The authors measured energy spectra in a sufficiently wide range of scattered particle energies at two initial energies of projectile ions: $E_0 = 5$ and 8 keV. Energy spectra were measured at the angle β values ranging from 25 to 85° with the step of 10°. The angles were counted from to the surface normal. The spectrometer energy resolution was $\Delta E/E = 0.019$.

To determine the potential parameters, the Zinoviev potential [6] and Moliere potential [1] with varying parameters were used. Finally, the best agreement with experiment was reached at a specific collision energy simultaneously for the entire set of experimental data.

The Zinoviev potential is defined as

$$U(R) = \frac{Z_1 Z_2 e^2}{R} \exp\{-B(x)x\},$$

$$B(x) = \frac{c_1}{1 + c_2 x^{1/2} + c_3 x}, \quad x = \frac{R}{a_f}.$$

Here Z_1 and Z_2 are the charges of colliding particles insert a space and remove the sign above the letter n nuclei, R is the internuclear distance. As screening length a_f, the parameter suggested by Firsov in [19] was used:

$$a_f = 0.88534 a_B \left(Z_1^{1/2} + Z_2^{1/2}\right)^{-2/3}, \quad a_B = 0.529\,\text{Å},$$

where a_B is the Bohr radius. .

The Moliere potential used in this study had the following form:

$$U(R) = \frac{Z_1 Z_2 e^2}{R} \sum_{i=1}^{3} c_i \exp\left(-d_i \frac{R}{a_f}\right).$$

Parameters ensuring the best fit to experiment are listed in Tables 1 and 2. In the case of the Moliere potential, parameters c_3 and d_3 did not affect the result because they describe interaction with the target K-shell, while distances relevant to this case were not achieved in the experiment under discussion.

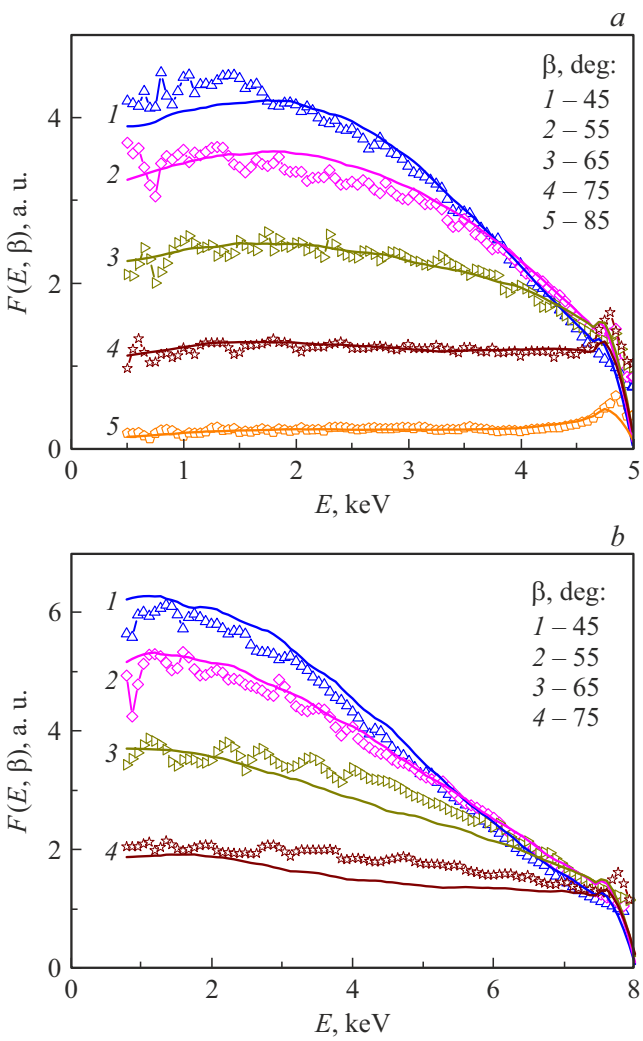

Figure 1. Intensities of scattered particles at collision energies $E_0 = 5$ (a) and 8 keV (b). Points represent experimental data from [18], lines demonstrate our calculations. β is the emission angle relative to the surface normal.

Fig. 1 illustrates the comparison between experimental and calculated spectra for different scattering angles and collision energies. For more clarity, the data are given only for a part of angles.

Potentials reconstructed from experimental data are presented in Fig. 2, *a*. As Fig. 2, *a* shows, the obtained values slightly depend on the used potential form, which confirms the method's remove the sign above the letter s reliability. We assumed that, when protons are scattered in a solid, an equilibrium beam distribution with respect to particle charges will be achieved, but it may be different at different initial energies. This is why the potential parameters at different energies were determined independently. One can see in Fig. 2, *a* that data obtained for different energies are close to each other, which once more confirms stability of the procedure for determining the potential parameters. Fig. 2, *a* demonstrates also the potential for gas–phase

collisions obtained by using the DFT method. One can see that the solid–phase collision potentials obtained in this study are considerably different from it.

Fig. 2, *b* presents screening function $B(R)$ for the cases shown in Fig. 2, *a*:

$$B(R) = -\ln\left[\frac{U(R)R}{Z_1 Z_2 e^2}\right]\frac{a_f}{R}.$$

Fig. 2, *b* shows that the obtained potentials are characterized by the screening function increase (with decreasing screening length) by 10–15% as compared with potentials that are used for gas–phase collisions. To our mind, this effect is caused by projectile–induced perturbations of electron gas density in metal. The increase in the electron gas density in the region between the projectile and scattering center causes enhancement of the interaction potential screening. Values of the gas–phase and solid–phase potentials become closer to each other with decreasing internuclear distance.

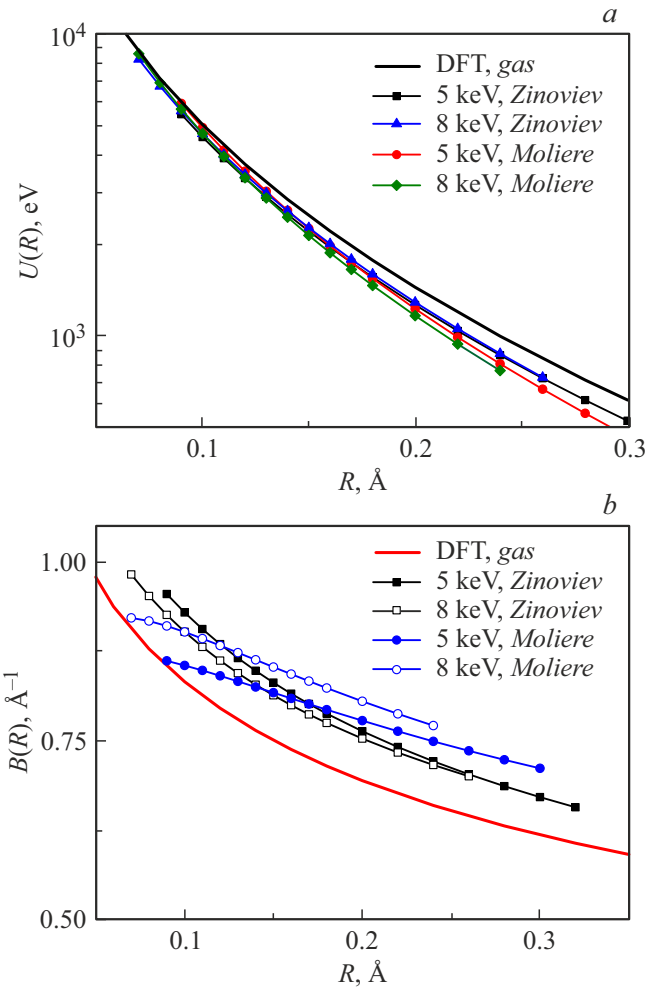

Figure 2. *a* — interatomic interaction potentials reconstructed from experimental data for different collision energies by using different potential formulae. The potential data are presented for the ranges of scattered atom energies observed in the experiment [18]. The DFT potential was calculated for gas–phase collisions. *b* — screening function $B(R)$ for the cases presented in panel *a*. The bold line represents the DFT potential for gas–phase collisions.

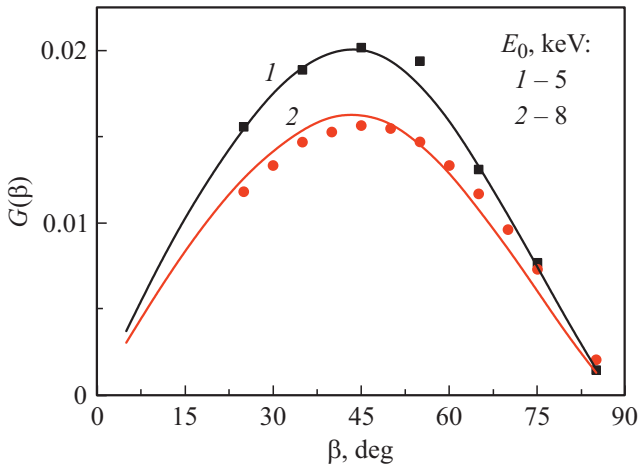

Figure 3. Angular distribution of backscattered hydrogen atoms with initial energies $E_0 = 5$ and 8 keV. Points are experimental data, lines are calculations.

One more criterion for properly choosing the interaction potential during computer simulation is coincidence of angular dependences of scattered particles with experimental data. Fig. 3 presents the angular distribution of backscattered hydrogen atoms integrated over all the output energies for initial energies $E_0 = 5$ and 8 keV. The ordinate axis presents function $G(\beta)$ defined as the number of reflected particles per incident proton and emission angle interval $\Delta\beta = 5°$:

$$G(\beta) = 4\pi \sin\left(\frac{\Delta\beta}{2}\right)\sin\beta \int_0^{E_0} F(E,\beta)dE.$$

Thus, in this study parameters of the potential for the ion–solid system were obtained from experimental data for the first time (using as an example experimental data on energy and angular distributions of backscattered particles during the golden target bombardment with protons). The obtained potential considerably differs from those used to describe gas–phase scattering and is characterized by a remarkable increase in the screening constant.

Financial support

Babenko, Mikhailov and Tensin thank you for the financial support the Russian Scientific Foundation (grant № 22-22-20081, https://rscf.ru/project/22-22-20081/) and also the Saint-Petersburg Scientific Foundation according to the agreement № 22/2022 of April 14, 2022.

Conflict of interests

The authors declare that they have no conflict of interests.

References

[1] G. Moliere, Z. Naturforsch. A., **2** (3), 133 (1947). DOI: 10.1515/zna-1947-0302

[2] J.F. Ziegler, J.P. Biersack, U. Littmark, *The stopping and range of ions in solids*. Ser.: Stopping and range of ions in matter (Pergamon, N.Y., 1985).

[3] W. Lenz, Z. Phys., **77** (11-12), 713 (1932). DOI: 10.1007/BF01342150

[4] H. Jensen, Z. Phys., **77** (11-12), 722 (1932). DOI: 10.1007/BF01342151

[5] W.D. Wilson, L.G. Haggmark, J.P. Biersack, Phys. Rev. B, **15** (5), 2458 (1977). DOI: 10.1103/PhysRevB.15.2458

[6] A.N. Zinoviev, Nucl. Instr. Meth. Phys. Res. B, **269** (9), 829 (2011). DOI: 10.1016/j.nimb.2010.11.074

[7] A.N. Zinoviev, K. Nordlund, Nucl. Instr. Meth. Phys. Res. B, **406** (Pt B), 511 (2017). DOI: 10.1016/j.nimb.2017.03.047

[8] D.S. Meluzova, P.Yu. Babenko, A.P. Shergin, K. Nordlund, A.N. Zinoviev, Nucl. Instr. Meth. Phys. Res. B, **460**, 4 (2019). DOI: 10.1016/j.nimb.2019.03.037

[9] A.N. Zinoviev, P.Yu. Babenko, K. Nordlund, Nucl. Instr. Meth. Phys. Res. B, **508**, 10 (2021). DOI: 10.1016/j.nimb.2021.10.001

[10] A. Agrawal, R. Mishra, L. Ward, K.M. Flores, W. Windl, Modelling Simul. Mater. Sci. Eng., **21** (8), 085001 (2013). DOI: 10.1088/0965-0393/21/8/085001

[11] C. Bjorkas, N. Juslin, H. Timko, K. Vortler, K. Nordlund, K. Henriksson, P. Erhart, J. Phys.: Condens. Matter, **21** (44), 445002 (2009). DOI: 10.1088/0953-8984/21/44/445002

[12] M.-C. Marinica, L. Ventelon, M.R. Gilbert, L. Proville, S.L. Dudarev, J. Marian, G. Bencteux, F. Willaime, J. Phys.: Condens. Matter, **25** (39), 395502 (2013). DOI: 10.1088/0953-8984/25/39/395502

[13] B. Bruckner, T. Strapko, M.A. Sortica, P. Bauer, D. Primetzhofer, Nucl. Instr. Meth. Phys. Res. B, **470**, 21 (2020). DOI: 10.1016/j.nimb.2020.02.018

[14] P.Yu. Babenko, D.S. Meluzova, A.P. Solonitsyna, A.P. Shergin, A.N. Zinoviev, JETP, **128** (4), 523 (2019). DOI: 10.1134/S1063776119030014.

[15] V.I. Shulga, Rad. Eff., **100** (1-2), 71 (1986). DOI: 10.1080/00337578608208737

[16] D.S. Meluzova, P.Yu. Babenko, A.P. Shergina, A.N. Zinoviev, J. Synch. Investig., **13** (2), 335 (2019). DOI: 10.1134/S1027451019020332.

[17] S.N. Markin, D. Primetzhofer, S. Prusa, M. Brunmayr, G. Kowarik, F. Aumayr, P. Bauer, Phys. Rev. B, **78** (19), 195122 (2008). DOI: 10.1103/PhysRevB.78.195122

[18] H. Verbeek, W. Eckstein, R.S. Bhattacharya, J. Appl. Phys., **51** (3), 1783 (1980). DOI: 10.1063/1.327740

[19] O.B. Firsov, Sov. Phys. JETP, **6** (3), 534 (1958).